Applied Catalysis B: Environmental 92 (2009) 377–383

Contents lists available at ScienceDirect

Applied Catalysis B: Environmental

journal homepage: www.elsevier.com/locate/apcatb

TiO_2 nanotubes and CNT–TiO_2 hybrid materials for the photocatalytic oxidation of propene at low concentration

N. Bouazza [a], M. Ouzzine [a], M.A. Lillo-Ródenas [a,*], D. Eder [b], A. Linares-Solano [a]

[a] Grupo de Materiales Carbonosos y Medio Ambiente, Dpto. Química Inorgánica, Facultad de Ciencias, Universidad de Alicante, Ap. 99, E-03080, Alicante, Spain
[b] Department of Materials Science and Metallurgy, University of Cambridge, New Museums Site, Pembroke Street, Cambridge CB23QZ, UK

ARTICLE INFO

Article history:
Received 7 April 2009
Received in revised form 4 August 2009
Accepted 22 August 2009
Available online 28 August 2009

Keywords:
Carbon nanotubes
TiO_2
Photocatalysis
Propene

ABSTRACT

In this work, we investigated titanium dioxide (TiO_2) nanotubes and CNT–TiO_2 hybrid materials for the photocatalytic oxidation (PCO) of propene at low concentration (100 ppmv) in gaseous phase. The materials were prepared via sol–gel method using sacrificial multi-walled carbon nanotubes (CNT) as templates and subsequent heat treatments to obtain the desired crystalline phase (anatase, rutile or a mixture of both) and eventually to remove the carbon template. We also studied rutile nanotubes for the first time and demonstrate that the activity strongly depends on the crystalline composition, following rutile < anatase < anatase/rutile mixture. The enhanced activity of the anatase–rutile mixture is attributed to the decrease in the electron–hole pair recombination due to the multiphasic nature of the particles. The key result of this work is the exceptional performance of the CNT–TiO_2 hybrid, which yielded the highest observed photocatalytic activity. The improved performance is attributed to synergistic effects due to the hybrid nature of the material, resulting in small anatase crystalline sizes (CNT act as heat sinks) and a reduced electron–hole pair recombination rate (CNTs act as electron traps). These results demonstrate the great potential of hybrid materials and stimulate further research on CNT-inorganic hybrid materials in photocatalysis and related areas.

1. Introduction

In the last decade, the synthesis of nanostructured TiO_2 materials has received a great deal of attention. Three approaches have been reported for the preparation of TiO_2-nanotube materials: the hydrothermal synthesis [1–7], the anodic oxidation [8–11] and the template synthesis [12–17]. The advantage of the template-based synthesis route is the straightforward control over the morphology of the resulting TiO_2 nanotubes. For instance, the initial dimensions of carbon nanotubes (CNTs) determine both, diameter and length of the TiO_2 nanotubes, while the TiO_2 nanotube wall thickness depends on the type and initial concentration of the Ti precursor with respect to the CNTs [15]. The use of CNTs as a template was further significant as they can also support the tubular morphology of TiO_2 during the phase transformation from anatase to rutile, resulting in the first synthesis of pure rutile nanotubes [16]. A significant innovation was the addition of small amounts of benzyl alcohol as a linking agent, which enabled the use of pristine CNTs as templates without the need for covalent functionalisation [17].

The last few years have seen a boost in interest in TiO_2 nanotubes, due to their improved performance as photocatalysts in heterogeneous photocatalysis [2,7,11,18–22]. However, most of these studies have been devoted to photocatalysis in solution and only the work of Inagaki et al. deals with gaseous phase oxidation [22]. According to some authors, the advantages of TiO_2 nanotubes are solely based on their high surface areas [2,18,19,23]. Other authors showed that TiO_2 nanotubes contain a high amount of hydroxyl groups in comparison with TiO_2 in the form of powder [6,24]. In general, nanotubes have a particular advantage in the way they enable three-dimensional mechanically coherent structures, which provide ready gas and radiation access to the material [14]. For example, Macak et al. [20] demonstrated that TiO_2 nanotubes showed higher photocatalytic activity than P25, despite their smaller surface area. Eder et al. investigated anatase nanotubes, both pure and doped with iron ions, for the photocatalytic splitting of water and observed that – in contrast to the inactive P25 – the TiO_2 nanotubes did produce a significant amount of hydrogen [21]. Both authors related this improvement to the structure of the TiO_2 nanotubes, which favours short diffusion paths of the pollutant molecules and, in addition, also decreases the electron–hole pair recombination velocity.

Despite these promising studies, the photocatalytic performance of TiO_2 nanotubes is far from completely understood. One important question involves the phase composition of TiO_2, which

* Corresponding author. Tel.: +34 965 909350; fax: +34 965 903454.
E-mail address: mlillo@ua.es (M.A. Lillo-Ródenas).

0926-3373/$ – see front matter © 2009 Elsevier B.V. All rights reserved.
doi:10.1016/j.apcatb.2009.08.017

has two main phases, anatase – typically formed upon synthesis – and rutile, the thermodynamically stable phase. Due to the synthesis conditions for rutile, which often require heat treatments at elevated temperatures (e.g. >600 °C), the crystal sizes in rutile are typically larger than in anatase, resulting in significantly smaller specific surface areas. The rutile nanotubes used in this work, however, have surface areas comparable with those of anatase nanotubes, and thus are ideal candidates for photocatalytic testing.

The test reaction in this work is the photocatalytic oxidation of volatile organic compounds (VOC) at low concentration, a very important catalytic process, with the aim to reduce their harmful effects for human health and environment. Among the different VOCs, this work concentrates on propene, which is one of the major sources of both outdoor (involved in vehicle emissions and in many industrial applications, such as in petrochemical plants and foundry operations) as well as of indoor (one of the principal components of tobacco smoke) air pollution. So far, very few studies have been reported on the photocatalytic oxidation (PCO) of propene in gas phase using TiO_2 [25–28] and to the best of our knowledge the performance of TiO_2 nanotubes has not been explored at all for this application or, in general, for gaseous phase applications.

In this respect, the novelty of this work is a detailed investigation of various TiO_2 nanotubes, consisting of either pure anatase or rutile, or of a mixture of anatase and rutile, for the photocatalytic oxidation (PCO) of propene. Furthermore, this work compares the best results obtained previously with hybrid TiO_2 catalysts (containing activated carbon [26] or MCM-41 [27]) with CNT–TiO_2 hybrids, a very promising new class of functional materials [29], and investigates the beneficial role of CNTs in photocatalysis.

2. Experimental

2.1. Photocatalysts preparation

The TiO_2 nanotubes used in this work were synthesised via a sol–gel process using sacrificial CNT as templates. Multi-walled carbon nanotubes (CNTs) were prepared by a modified chemical vapor deposition (CVD) process, using ferrocene as the catalyst precursor and toluene as the feedstock. These reactants were vaporised into a hydrogen/argon atmosphere at 760 °C. The average outer diameter of the nanotubes was 70 nm and the length was between 20 and 30 μm, but can be controlled by adjusting various process parameters. Prior to their use as a template, amorphous carbon as well as residual iron catalyst particles were removed by annealing the as-grown CNTs in argon at 2000 °C for 5 h [29]. The synthesis of the CNT–TiO_2 hybrids and the TiO_2 nanotubes is described in detail elsewhere [14,16]. In summary, it involves (I) the deposition of a layer of TiO_2 synthesised by means of the sol–gel method on CNTs with the aid of benzyl alcohol as a linking agent, (II) heat treatment in argon to obtain the desired crystalline phases, e.g. anatase (350 °C), anatase–rutile mixture (550 °C) or rutile (700 °C), and (III) heat treatment in air at 520 °C to remove the CNT templates.

2.2. Characterisation techniques

The porosity characterisation of the TiO_2 nanotubes was performed by nitrogen adsorption at −196 °C, using an ASAP 2020 apparatus from Micromeritics. The specific surface area was measured by N_2 adsorption according to Brunauer–Emmett–Teller (BET).

X-ray powder diffraction was performed to characterise the phase composition and crystal structure of the photocatalysts, using a SEIFERT 2002 equipment as well as a Bruker D8 Advance (40 kV/40 mA) with Cu Kα (1.54 Å) radiation. The scanning velocity was 2°/min, and the 2θ range scanned ranged from 2° to 80°. The percentages of anatase and rutile were determined by using the intensities of the strongest peaks for anatase and rutile following the equations [26]:

$$W_R\ (\%) = \frac{A_R}{0.8844A_A + A_R} \times 100 \quad (1)$$

$$W_R\ (\%) + W_A\ (\%) = 100 \quad (2)$$

where W_A: composition percentage of anatase; W_R: composition percentage of rutile; A_A: integrated intensity of the maximum intensity peak of anatase (1 0 1); A_R: integrated intensity of the maximum intensity peak of rutile (1 1 0).

The crystalline sizes of the anatase and rutile phases were determined by the Scherrer formula, using a K factor of 0.93:

$$B = \frac{K\lambda}{\beta \cos\theta} \quad (3)$$

where B: crystalline size, in nm; λ: wavelength for the radiation used, which is 1.54056 Å for Cu; β: full width at half maximum intensity (FWHM); θ: angle for the XRD maximum peak.

The morphology of the samples was characterised by (i) scanning electron microscopy (SEM), using a JEOL 6340F FEG-SEM, and (ii) transmission electron microscopy (TEM) using INCA Energy TEM100 equipment from OXFORD instruments.

2.3. Experimental conditions for propene oxidation at low concentration

The experimental system used in propene PCO tests was designed in our laboratory. It consists of a quartz reactor (cut-off < 200 nm) where the photocatalyst bed is placed on quartz wool. The reactor is 50 mm height, its diameter is 20 mm and the quartz wool support height is around 10 mm. An 8 W Philips UV lamp is placed parallel to the quartz reactor, at around 1 cm. The UV lamp radiation peak appears at 257.7 nm (UV-C). The commercial reference of the lamp is TUV 8W FAM. The couple quartz reactor-lamp is surrounded by a cylinder covered by tinfoil. A scheme of this system is detailed elsewhere [26].

The weight of photocatalyst used in these experiments was 0.11 g for the TiO_2 nanotubes and, for comparison purposes, 0.16 g of the CNT–TiO_2 sample were used, maintaining a similar weight of TiO_2. The photocatalysts were used for the oxidation of propene at 100 ppm in air at room temperature, 25 °C.

Different flow rates of the propene stream, 7.5, 30 and 60 ml/min (STP), were tested. These flow rates were controlled by automated mass flow-controllers (Brook Instruments).

After suitable calibrations, a mass spectrometer (Balzers, Thermostar GSD 301 01) coupled to the outlet of the reactor bed follows the evolution of the concentration of propene in the outlet gas with time. The experiments were repeated at least two times for checking reproducibility.

Propene conversion was calculated using the following expression:

$$\text{Propene conversion}\ (\%) = \frac{C_{\text{initial } C_3H_6} - C_{\text{stationary } C_3H_6}}{C_{\text{initial } C_3H_6}} \times 100$$

where $C_{\text{initial } C_3H_6}$ is the initial propene concentration, 100 ppmv, and $C_{\text{stationary } C_3H_6}$ is the stationary propene concentration in the photocatayst bed outlet gas when the UV is switched on.

The standard activity of different samples was determined by using the following equation:

$$\text{St. activity} = \frac{n}{m \cdot t}$$

where St. activity: standard activity (mol/g min); n: moles of the propene oxidised; m: mass of the TiO_2-based sample (g); t: reaction time (min).

The standard activity related to surface area for all samples studied was determined by the following equation:

$$SAR_{S_{BET}} = \frac{\text{St. activity}}{S_{BET}}$$

where $SAR_{S_{BET}}$: standar activity related to surface area (mol/m^2 min); St. activity: standard activity related (mol/g min); S_{BET}: surface area (m^2/g).

The amount of CO_2 after the oxidation was quantified by mass spectrometry, using a calibrated CO_2-cylinder with a concentration of 300 ppmv.

3. Results and discussion

3.1. Photocatalysts preparation and characterisation

3.1.1. Nomenclature

X-ray diffraction (XRD) analysis of the as-prepared samples revealed that the TiO_2 coating on CNTs in the as-prepared samples was amorphous and thus required heat treatments (shown in Table 1) to induce crystallisation and phase transformation [15]. From the pristine material, several samples were prepared. The first sample (CNT–TiO_2) was simply obtained heating in argon at 350 °C, at which the amorphous phase crystallised into anatase without removing the CNTs, as confirmed by XRD in Fig. 1. The content of TiO_2 and CNTs of this hybrid sample is calculated to be 70% and 30% by weight, respectively.

Sample TiO_2-NT1 was prepared from the pristine material by a heat treatment in air at 520 °C to remove the carbon nanotubes.

By heating the sample in argon at higher temperatures, the anatase was transformed into rutile either partially (at 550 °C) or completely (at 700 °C). Sample TiO_2-NT2 was prepared by heat treatment in Ar at 550 °C followed by a heat treatment in air at 520 °C. Sample TiO_2-NT3 was prepared by heat treatment in Ar at 700 °C followed by a heat treatment in air at 520 °C.

XRD analysis showed that the heat treatment in air at 520 °C, required to remove the CNT template, did not affect the phase composition of the samples (Fig. 1).

The temperatures of heat treatment in Ar used to prepare the TiO_2-NT2 and TiO_2-NT3 samples were selected with the purpose of studying the effect of the crystalline composition (anatase/rutile) in the catalytic activity. In addition, the effect of the presence of the carbon nanotubes in the CNT–TiO_2 hybrid has been analysed.

3.1.2. Crystalline phase characterisation

Fig. 1 shows the XRD pattern of the investigated samples and reveals various crystal structures. The observed diffractions in sample CNT–TiO_2 are typical for the anatase phase, and their broadness suggests the presence of very small crystals. The peak at a 2θ of 26.4° is typical for the 0 0 2 diffraction of graphite [30] and confirms the presence of CNTs in the sample. Note, there are no traces of rutile in this sample.

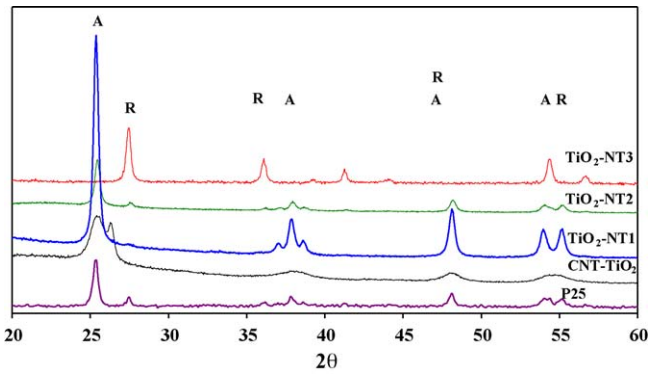

Fig. 1. XRD patterns of some TiO_2 nanotubes used in this study together with P25, used as reference. A: anatase; R: rutile.

Table 2
Characterisation of the composition and morphology of the crystalline phases of TiO_2, determined by XRD.

Samples	W_A (%)	B_A (nm)	W_R (%)	B_R (nm)
P25	70	20.2	30	30.8
CNT–TiO_2	100	5.3	–	–
TiO_2-NT1	100	23.4	–	–
TiO_2-NT2	72	23.8	28	23.7
TiO_2-NT3	–	–	100	24.0

The TiO_2-nanotube samples were heated in air at 520 °C in order to remove the CNT template, as confirmed by the absence of the d-0 0 2 diffraction in the corresponding XRD pattern. Similar to CNT–TiO_2, sample TiO_2-NT1 only shows the presence of anatase crystals. Apparently, the heat evolution during the oxidation of CNTs did not induce significant phase transformation. The peak widths, however, are much smaller than those in sample CNT–TiO_2, indicating a significant grain growth. In contrast, samples TiO_2-NT2 and TiO_2-NT3 were both heat-treated in argon at elevated temperatures prior to the oxidation of CNTs. The corresponding pattern shows diffractions typical for rutile. Heat treatment at 550 °C converted the anatase phase only partially (TiO_2-NT2), while the TiO_2-NT3 sample contained only the rutile phase. For comparison, the reference sample Degussa-P25 showed a similar anatase–rutile mixture as TiO_2-NT2.

The percentages of anatase and rutile and the corresponding crystal sizes are summarised in Table 2.

As indicated above, the CNT–TiO_2 sample contained only anatase, while the various heat treatments changed the phase composition from 100% anatase (TiO_2-NT1), to 72% anatase and 28% rutile (TiO_2-NT2) and finally 100% rutile (TiO_2-NT3).

It appears that the crystal sizes of the anatase phase for most TiO_2-nanotubes samples were similar to that in P25, except in the case of CNT–TiO_2, which contained anatase crystals with an average size of 5 nm. The average crystal sizes of rutile in TiO_2-NT2 and TiO_2-NT3 are also smaller than in P25. This is in line with our previous observations, which suggested that CNTs stabilize small

Table 1
Summary of the nomenclature and some characteristics of TiO_2 nanotubes.

Sample	Temperature of treatment (°C) in air	Temperature of treatment (°C) in Ar	Quantity of TiO_2 (%)	Quantity of CNT (%)	Phase composition	S_{BET} (m^2/g)
P25	–	–	100	–	Anatase–rutile	54
CNT–TiO_2	–	350	70	30	Anatase	22
TiO_2-NT1	520	–	100	–	Anatase	12
TiO_2-NT2	520	550	100	–	Anatase–rutile	13
TiO_2-NT3	520	700	100	–	Rutile	27

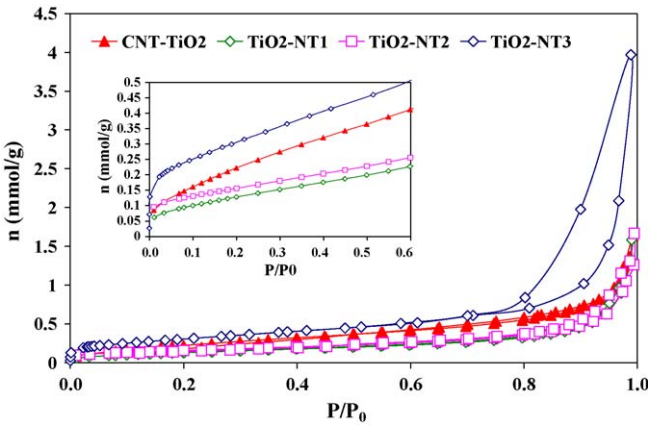

Fig. 2. Nitrogen adsorption isotherms at −196 °C of TiO_2 nanotubes.

crystal sizes during crystallisation and phase transformation treatments [15].

3.1.3. Porous texture

The porous texture characterisation of the samples was performed by N_2 adsorption at −196 °C. Fig. 2 shows the adsorption isotherms of nitrogen at −196 °C of the TiO_2 nanotubes, TiO_2-NT1, TiO_2-NT2, and TiO_2-NT3, as well as that for the CNT–TiO_2 hybrid.

The results confirm that the N_2 adsorption isotherms are of type II for all samples and that the elimination of the CNTs caused a decrease in porosity. The specific surface areas of the TiO_2 nanotubes are in the range between 12 and 27 m^2/g and thus smaller than the surface area of TiO_2 P25-Degussa (54 m^2/g). Interestingly, the surface area of the rutile nanotube is larger that for both the anatase and anatase–rutile nanotubes. This is attributed to the presence of benzyl alcohol and CNTs, both of which prevent grain growth during phase transformation and so stabilize very small particles [15,17]. By adjusting process parameters and choice of CNTs, rutile nanotubes with surface areas as larges as 60–80 m^2/g could be produced [15,16]. The surface area for the sample studied in this work (27 m^2/g) is still considerably larger than most commercial samples of unsupported rutile materials [31,32].

3.1.4. Morphology

The samples were investigates with both, transmission electron microscopy (TEM) and scanning electron microscopy (SEM).

TEM image in Fig. 3 presents the CNT–TiO_2 and TiO_2-NT2 samples, from which the size of the TiO_2 particles can be determined. In Fig. 3a the part of CNT covered by TiO_2 shows a complete covering of TiO_2. The nanosized TiO_2 supported on the CNT is observed to be homogeneously and densely spread on the surfaces of the CNT. Fig. 3b allows to clearly observe TiO_2 nanotubes resulting from the grown on a carbon nanotube and its subsequent burning. In this case, the diameter of TiO_2 in TiO_2-NT2 nanotube is around 100 nm.

The SEM image in Fig. 4a shows a smooth, uniform coating of CNTs with TiO_2, indicating small crystal sizes. The outer diameter ranges from 80 to 150 nm, which corresponds to a wall thickness of 20–40 nm. The occasional presence of fractures is attributed to the vacuum assisted drying process. Fig. 4b shows the corresponding SEM images for the TiO_2 nanotubes and reveal that the CNTs have indeed been removed upon oxidation, as suggested from XRD analysis, while preserving the tubular morphology. The cylinder hole, around 50 nm, is clearly observed [15]. The walls consist of

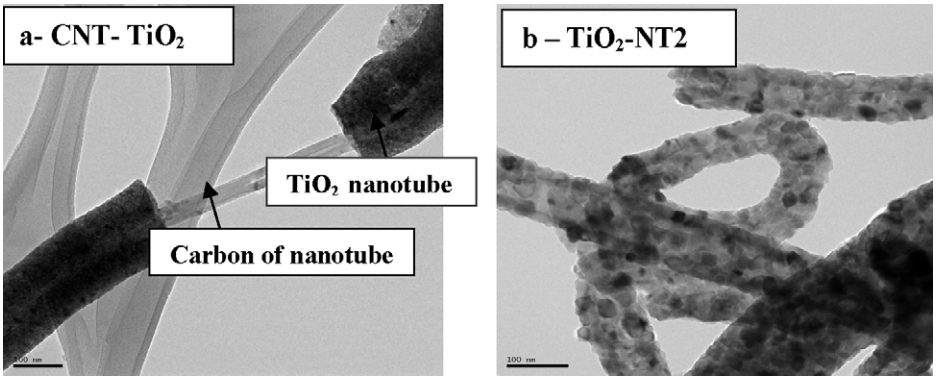

Fig. 3. TEM micrographs images of (a) CNT–TiO_2 hybrid and (b) TiO_2-NT2 (in all images the bar corresponds to 100 nm).

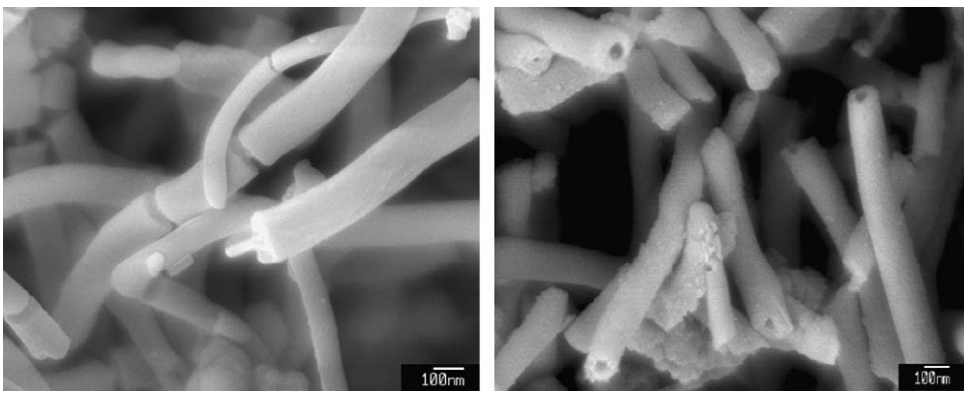

Fig. 4. SEM images of (a) CNT–TiO_2 hybrid and (b) TiO_2-NT2.

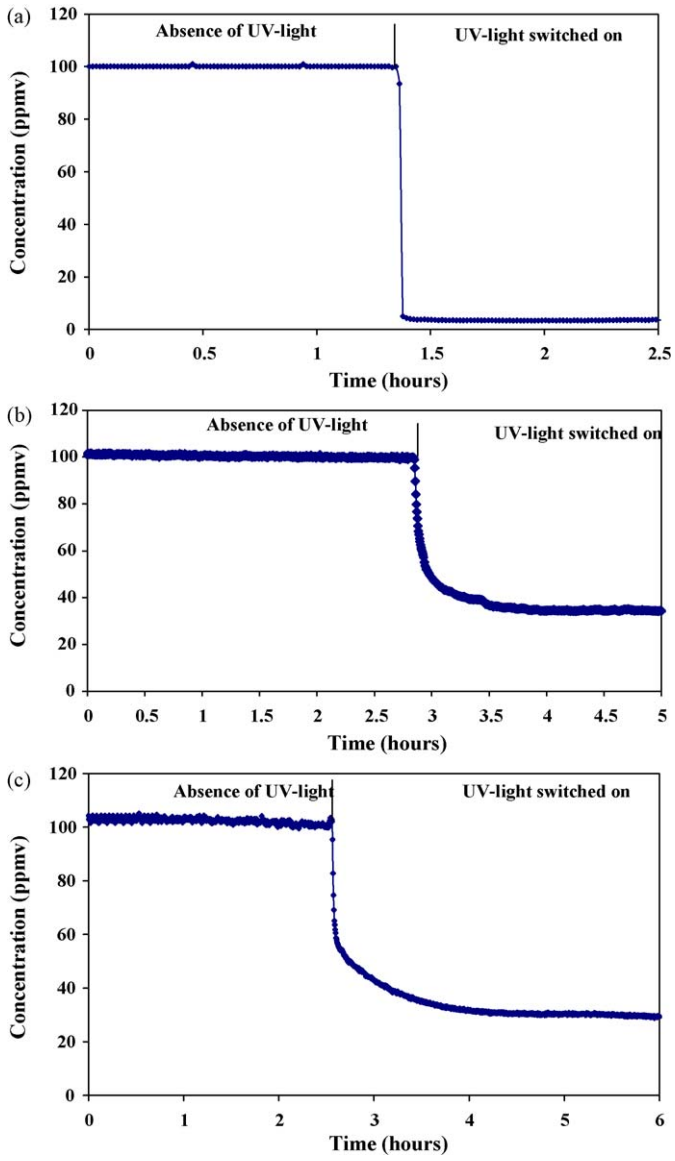

Fig. 5. Photocatalytic activity for the oxidation of propene at 7.5 ml/min using UV-light (peak wavelength 257.7 nm) for photocatalysts: (a) P25, (b) TiO_2-NT1 and (c) CNT–TiO_2.

crystals with sizes of about 20 nm, close to the average values obtained by XRD.

3.2. Activity of the photocatalysts for propene oxidation at low concentration

The photocatalytic performance of these new materials was investigated for the oxidation of propene at low concentration, 100 ppmv, using different flow rates, 7.5, 30 and 60 ml/min. After a certain time in the dark to allow equilibrium adsorption, the samples were illuminated using a UV lamp with a radiation peak at 257.7 nm. The weight of the samples was 0.11 g for TiO_2 nanotubes, while 0.16 g was chosen for the CNT–TiO_2 sample (70% TiO_2 and 30% of carbon nanotubes) so that the weight of TiO_2 was constant in all experiments. The fact that the weight ratio carbon/TiO_2 is 30/70 lets us compare the obtained results with those of other hybrids previously studied, containing the same ratio [26,27].

Table 3
Propene conversion by P25 and the TiO_2-nanotube photocatalysts using different 100 ppmv propene stream flow rates.

Samples	Conversion at 7.5 ml/min	Conversion at 30 ml/min	Conversion at 60 ml/min
P25	100	78	50
CNT–TiO_2	71	41	38
TiO_2-NT1	65	21	14
TiO_2-NT2	69	25	16
TiO_2-NT3	45	13	7

3.2.1. Oxidation of propene using TiO_2 nanotubes

Each experiment was performed by passing the propene stream through the photocatalyst bed until the propene concentration in the outlet stream equalled the inlet concentration. Then, the UV-light was switched on and the decrease in the propene concentration over time was recorded, as shown in Fig. 5 for P25, TiO_2-NT3 and CNT–TiO_2. The performance of the other TiO_2 nantube samples was similar to TiO_2-NT3.

The results of Fig. 5a–c, shows as an example of all the samples studied, indicate that the propene adsorption on the surface of TiO_2 before UV illumination was negligible for both the commercial sample and the TiO_2 nanotubes. After switching on the UV source, the propene concentration in the outlet stream of the reactor decreased rapidly, though significantly at a slower rate for the TiO_2 nanotubes compared with P25. Thus, the reaction rates for the photocatalytic oxidation are lower for the nanotubes than for P25.

The results for the conversion of propene at 100 ppmv and the calculated activities are shown in Tables 3 and 4, respectively, for three different flow rates: 7.5, 30 and 60 ml/min.

At first glance, it appears that all TiO_2 nanotubes are considerably less active than the P25. This, however, can be explained by the significantly smaller surface area of the nanotubes as shown by the activity related to surface area.

Both, conversion and activity depend on the phase composition of the TiO_2 catalysts. The results shows that the rutile nanotubes, depite their comparatively higher surface areas, performed less than the anatase nanotubes. The performance was significantly improved in the sample which contained a mixture of anatase and rutile. The highest activity was, however, observed in the CNT–TiO_2 hybrid, thus suggesting a synergistic role of CNTs.

Thus, the main conclusions, according to Table 4 and Fig. 6 are the following:

Table 4
Standard activity per gram of sample (st. activity) or related to surface area ($SAR_{S_{BET}}$) for all samples studied at three flows, 7.5, 30 and 60 ml/min.

Samples	7.5 ml/min		30 ml/min		60 ml/min	
	St. activity (mol/g min)	$SAR_{S_{BET}}$ (mol/m^2 min)	St. activity (mol/g min)	$SAR_{S_{BET}}$ (mol/m^2 min)	St. activity (mol/g min)	$SAR_{S_{BET}}$ (mol/m^2 min)
CNT–TiO_2	1.36×10^{-7}	6.18×10^{-9}	3.15×10^{-7}	14.32×10^{-9}	5.83×10^{-7}	26.50×10^{-9}
TiO_2-NT1	1.81×10^{-7}	15.08×10^{-9}	2.34×10^{-7}	19.50×10^{-9}	3.12×10^{-7}	26.00×10^{-9}
TiO_2-NT2	1.92×10^{-7}	14.77×10^{-9}	2.80×10^{-7}	21.54×10^{-9}	3.57×10^{-7}	27.46×10^{-9}
TiO_2-NT3	1.25×10^{-7}	4.63×10^{-9}	1.45×10^{-7}	5.37×10^{-9}	1.56×10^{-7}	5.78×10^{-9}
P25	2.80×10^{-7}	5.18×10^{-9}	8.70×10^{-7}	16.11×10^{-9}	1.17×10^{-6}	21.67×10^{-9}

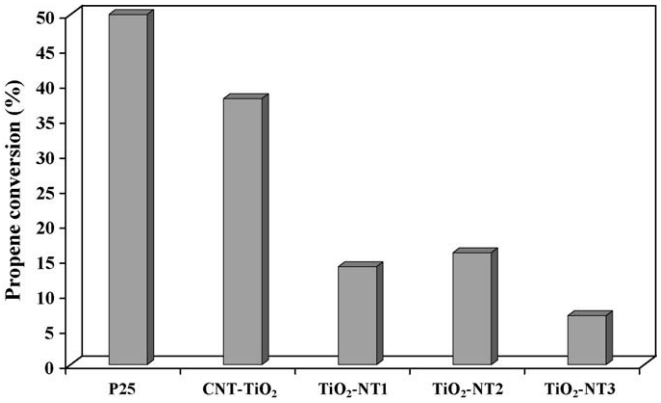

Fig. 6. Oxidation of propene using 60 ml/min flow rate for the all photocatalysts.

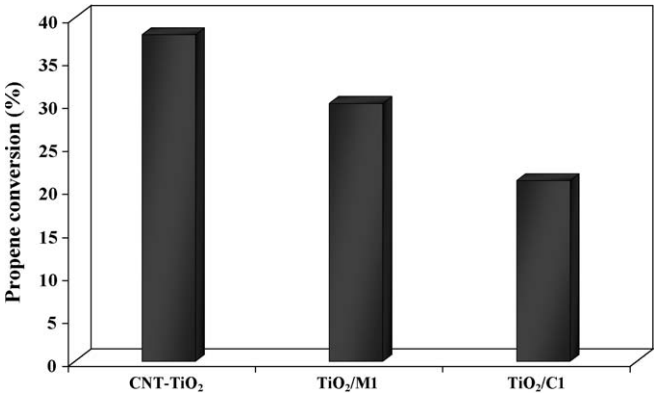

Fig. 7. Propene oxidation using 60 ml/min flow rate for the three hybrids.

(a) The difference in performance between the anatase and rutile nanotubes was observed for all three flow rates and was most dominant at a flow rate of 60 ml/min. As XRD analysis confirmed, the crystal size for anatase in TiO_2-NT1 is similar to that of rutile in TiO_2-NT3, thus the crystal size is not responsible for the observed difference. This observation is even more interesting, if one considers that the BET surface area of the rutile sample is more than twice that of the anatase sample. Hence, the considerably lower photocatalytic activity seems to origin solely in the electronic or structural nature of the rutile phase. This result is in agreement with some studies, which indicated that the anatase phase has a larger photocatalytic activity than the rutile phase [33,34]. The authors related the superior activity of the anatase phase to its better adsorption capacity of organic compounds and, more likely, to its slower recombination rate of the hole–electron pairs [33,34]. However, most of these studies used rutile materials that had significantly smaller surface areas than the anatase materials. Therefore, an effect of the surface area could not be entirely excluded, in contrast to our work, which compared a rutile material with a larger surface area than anatase.

(b) Interestingly, sample TiO_2-NT2 exhibited a photocatalytic activity that was even higher than that of the anatase nanotubes. From XRD analysis it is known that this sample contains a mixture of anatase (72%) and rutile (28%). This ratio is similar to that of P25, one of the most frequently studied TiO_2 materials. The Standard activity related to surface area of this sample should also be remarked, and its excellent photocatalytic performance has been attributed to an enhanced separation of hole–electron pairs caused by the multiphase nature containing anatase and rutile [34,35].

(c) The most intriguing result is the performance of the CNT–TiO_2 hybrid, which showed the highest conversion and activity values of the investigated samples. This sample consists of 70% TiO_2 (100% anatase) and 30% CNTs.

There are several possible explanations for the synergistic role of CNTs, depending on the inorganic material and choice of application.

(1) The first explanation is purely physical and can be described in terms of CNT acting as a dispersing agent which prevents TiO_2 from agglomerating, thus providing a higher active surface area of the resulting catalyst compared with the single phase TiO_2. In our work, the crystal size of anatase in this sample was significantly smaller (5 nm) when supported on CNTs than those in the nanotube samples NT1 and NT2 (23 nm). The beneficial role of CNTs in this scenario would be their high specific surface area as well as their high thermal conductivity, which enable the use of CNTs as a support and heat sink during heat treatments, thus stabilizing small particle sizes [29].

(2) Another explanation is the synergistic role of CNTs based on charge transfer processes between CNTs and TiO_2. CNTs are excellent electrical conductors and can so either provide (CNTs as photosensitizers) or accept (CNTs as electron sinks) electrons, which are transferred through the CNT–TiO_2 interface [29]. For instance, electrons can be photo-induced in CNTs and easily transferred to the CNT–TiO_2 interface, where they are injected into the TiO_2 conduction band. These electrons can trigger the formation of very reactive radicals such as superoxide radical ions ($O_2^{\bullet -}$) and hydroxyl radicals ($HO^{\bullet}$), which are then responsible for the degradation of the organic compound. A similar electron transfer was observed between various other carbon materials and the TiO_2 semiconductor [36].

Alternatively, the charge transfer direction can also be reverted, so that CNTs act as an electron acceptor, promoting interfacial electron-transfer processes from the attached oxide to the CNT. This results in a separation of charges, which retards the recombination of photo-induced electrons and holes and hence improves the photocatalytic activity of the semiconductor.

To distinguish between these effects, the CNT–TiO_2 hybrid was compared with hybrid TiO_2 photocatalysts, containing MCM-41 (TiO_2/M1) [27] or activated carbon (TiO_2/C1) [26,27]. Both of these supports have very high surface areas, which can stabilize small crystal sizes, but do not exhibit electrical properties as good as CNTs. Fig. 7 shows the catalytic activity of three photocatalysts CNT–TiO_2, TiO_2/M1 and TiO_2/C1.

In spite of the different morphology of these hybrids (CNT–TiO_2 is in form of powder and TiO_2/M1 and TiO_2/C1 are in form of pellets), it is possible to observe that the CNT–TiO_2 hybrid shows the highest photocatalytic activity amongst the three.

The amount of CO_2 generated as an oxidation propene has been quantified and compared with the oxidised propene. Thus, the ratio mol of CO_2 generated/mol of propene oxidised is around 3 in all the experiments, which indicated total mineralisation of the oxidised propene to carbon dioxide and water, according to previously published results dealing with propene oxidation [25,28]. As an example, this ratio mol of CO_2 generated/mol of propene oxidised is 2.75 for propene oxidation at 60 ml/min for sample TiO_2-NT1.

The previously obtained results remark the important role played by morphology of the nanotubes, and highlight the novelty of this work on hybrids. This aspect will be studied in depth in the future.

4. Conclusions

The present paper has studied the photocatalytic oxidation of propene at low concentration (100 ppm) using titanium dioxide

nanotubes. The results of this study allow obtaining the following conclusions.

Nitrogen adsorption shows that all these TiO_2 materials are macroporous, as the commercial TiO_2 photocatalyst (Degussa-P25). The use of XRD and TEM techniques has shown that the different TiO_2-nanotube samples have different crystalline structures, with different anatase and rutile percentages.

Comparison between the photocatalytic activities of TiO_2 nanotubes allows concluding that the differences in activity are related to two factors. One of them is the percentage of the two phases, anatase and rutile, of TiO_2. Thus, the TiO_2-NT2 photocatalyst, which contains 72% of anatase and 28% of rutile, is the best one.

The other is the composition, especially the carbon content. Thus, the CNT–TiO_2 photocatalyst, which contains in its composition 70% of TiO_2 and 30% of CNT, shows the highest photocatalytic activity, higher than that for TiO_2-NT2.

Total mineralisation of the oxidised propene to carbon dioxide and water has been obtained in the oxidation experiments for all photocatalysts studied.

The activity of the CNT–TiO_2 hybrid is larger than that of other hybrid TiO_2 photocatalysts previously studied, what remarks the importance of the electric properties of the hybrid and interesting morphology.

Acknowledgements

The authors thank MCYT (CTQ2005-01358/PPQ) and Generalitat Valenciana (ARVIV 2007/063 and Prometeo/2009/047) for financial support. M. Ouzzine thanks MAEC-AECID for a predoctoral fellowship.

References

[1] B.D. Yao, Y.F. Chan, X.Y. Zhang, W.F. Zhang, Z.Y. Yang, N. Wang, Appl. Phys. Lett. 82 (2) (2003) 281–283.
[2] G. Zhanqi, Y. Shaogui, T. Na, S. Cheng, J. Hazard. Mater. 145 (2007) 424–430.
[3] M. Qamar, C.R. Yoon, H.J. Oh, N.H. Lee, K. Park, D.H. Kim, K.S. Lee, W.J. Lee, S.J. Kim, Catal. Today 131 (2008) 3–14.
[4] C.-C. Tsai, H. Teng, Chem. Mater. 18 (2006) 367–373.
[5] M.A. Khan, H.-T. Jung, O.-B. Yang, J. Phys. Chem. B 110 (13) (2006) 6626–6630.
[6] T. Kasuga, Thin Solid Films 496 (2006) 141–145.
[7] K. Byrappa, A.S. Dayananda, C.P. Sajan, B. Basavalingu, M.B. Shayan, K. Soga, M. Yoshimura, J. Mater. Sci. 43 (2008) 2348–2355.
[8] Y.S. Sohn, Y.R. Smith, M. Misra, V. Subramanian, Appl. Catal. B: Environ. 84 (2008) 372–378.
[9] P. Hoyer, Langmuir 12 (1996) 1411–1413.
[10] D. Gong, C.A. Grimes, O.K. Varghese, J. Mater. Res. 16 (12) (2001) 3331–3334.
[11] H.-C. Liang, X.-Z. Li, J. Hazard. Mater. 162 (2009) 1415–1422.
[12] A. Jitianu, T. Cacciaguerra, M.H. Berger, R. Benoit, F. Béguin, S. Bonnamy, J. Non-Cryst. Solids 345/346 (2004) 596–600.
[13] H. Imai, Y. Takei, K. Shimizu, M. Matsuda, H. Hirashima, J. Mater. Chem. 9 (1999) 2971–2972.
[14] D. Eder, M.S. Motta, I.A. Kinloch, A.H. Windle, Physica E 37 (2007) 245–249.
[15] D. Eder, A.H. Windle, J. Mater. Chem. 18 (2008) 2036–2043.
[16] D. Eder, I.A. Kinloch, A.H. Windle, Chem. Commun. (2006) 1448–1450.
[17] D. Eder, A.H. Windle, Adv. Mater. 20 (2008) 1787–1793.
[18] Y.-Y. Hsu, T.-L. Hsiung, H.P. Wang, Y. Fukushina, Y.-L. Wei, J.-E. Chang, Mar. Pollut. Bull. 57 (2008) 873–876.
[19] L.-R. Hou, C.Z. Yuan, Y. Peng, J. Hazard. Mater. B 139 (2007) 310–315.
[20] J.M. Macak, M. Zlamal, J. Krysa, P. Schmuki, Small 3 (2) (2007) 300–304.
[21] D. Eder, M.S. Motta, A.H. Windle, Nanotechnology 20 (5) (2009) 055602.
[22] M. Inagaki, N. Kondo, R. Nonaka, E. Ito, M. Toyoda, K. Sogabe, T. Tsumura, J. Hazard. Mater. 161 (2–3) (2009) 1514–1521.
[23] G. Zhanqi, Y. Shaogui, S. Cheng, H. Jun, Sep. Purif. Technol. 58 (2007) 24–31.
[24] T. Kasuga, M. Hiramatsu, A. Hoson, T. Sekino, K. Niihara, Adv. Mater. 11 (15) (1999) 1307–1311.
[25] C.T. Brigden, S. Poulston, M.V. Twigg, A.P. Walker, A.J.J. Wilkins, Appl. Catal. B: Environ. 32 (1–2) (2001) 63–71.
[26] M.A. Lillo-Ródenas, N. Bouazza, A. Berenguer-Murcia, J.J. Linares-Salinas, P. Soto, A. Linares-Solano, Appl. Catal. B: Environ. 71 (3–4) (2007) 298–309.
[27] N. Bouazza, M.A. Lillo-Ródenas, A. Linares-Solano, Appl. Catal. B 77 (2008) 284–293.
[28] N. Bouazza, M.A. Lillo-Ródenas, A. Linares-Solano, Appl. Catal. B: Environ. 84 (2008) 691–698.
[29] D. Eder, Chem. Rev., accepted for publication.
[30] H.O. Pierson, Handbook of Carbon, Graphite, Diamonds and Fullerenes: Processing, Properties and Applications, 1st ed., Noyes Publications, Park Ridge, 1993.
[31] D. Eder, R. Kramer, Phys. Chem. Chem. Phys. 5 (6) (2003) 1314–1319.
[32] D. Eder, R. Kramer, J. Phys. Chem. B 108 (39) (2004) 14823–14829.
[33] A.-C. Lee, R.-H. Lin, C.-Y. Yang, M.H. Lin, W.-Y. Wang, Mater. Chem. Phys. 109 (2008) 275–280.
[34] D.C. Hurum, A.G. Agrios, K.A. Gray, J. Phys. Chem. B 107 (19) (2003) 4545–4549.
[35] O. Carp, C.L. Huisman, A. Reller, Prog. Solid State Chem. 32 (1–2) (2004) 33–177.
[36] H.-C. Huang, G.-L. Huang, H.-L. Chen, Y.-D. Lee, Thin Solid Films 511/512 (2006) 203–207.